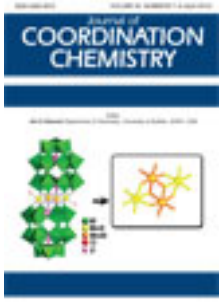

Journal of Coordination Chemistry
Publication details, including instructions for authors and subscription information:
http://www.tandfonline.com/loi/gcoo20

Synthesis, characterization, crystal structure, and DNA-binding of ruthenium(II) complexes of heterocyclic nitrogen ligands resulting from a benzimidazole-based quinazoline derivative

H. Paul [a], T. Mukherjee [a], M.G.B. Drew [b] & P. Chattopadhyay [a]
[a] Department of Chemistry, Burdwan University, Golapbag, Burdwan-713104, India
[b] Department of Chemistry, Reading University, Reading RG6 6AD, Berks, England
Published online: 21 Mar 2012.

To cite this article: H. Paul, T. Mukherjee, M.G.B. Drew & P. Chattopadhyay (2012) Synthesis, characterization, crystal structure, and DNA-binding of ruthenium(II) complexes of heterocyclic nitrogen ligands resulting from a benzimidazole-based quinazoline derivative, Journal of Coordination Chemistry, 65:8, 1289-1302, DOI: 10.1080/00958972.2012.667807

To link to this article: http://dx.doi.org/10.1080/00958972.2012.667807

Journal of Coordination Chemistry
Vol. 65, No. 8, 20 April 2012, 1289–1302

Synthesis, characterization, crystal structure, and DNA-binding of ruthenium(II) complexes of heterocyclic nitrogen ligands resulting from a benzimidazole-based quinazoline derivative

H. PAUL†, T. MUKHERJEE†, M.G.B. DREW‡ and P. CHATTOPADHYAY*†

†Department of Chemistry, Burdwan University, Golapbag, Burdwan-713104, India
‡Department of Chemistry, Reading University, Reading RG6 6AD, Berks, England

(*Received 30 November 2011; in final form 25 January 2012*)

The reaction of *cis*-[$RuCl_2(dmso)_4$] with [6-(2-pyridinyl)-5,6-dihydrobenzimidazo[1,2-c] quinazoline] (**L**) afforded in pure form a blue ruthenium(II) complex, [$Ru(L^1)_2$] (**1**), where the original **L** changed to [2-(1H-benzoimidazol-2-yl)-phenyl]-pyridin-2-ylmethylene-amine (**HL^1**). Treatment of $RuCl_3 \cdot 3H_2O$ with L in dry tetrahydrofuran in inert atmosphere led to a green ruthenium(II) complex, *trans*-[$RuCl_2(L^2)_2$] (**2**), where **L** was oxidized *in situ* to the neutral species 6-pyridin-yl-benzo[4,5]imidazo[1,2-c]quinazoline (**L^2**). Complex **2** was also obtained from the reaction of $RuCl_3 \cdot 3H_2O$ with L^2 in dry ethanol. Complexes **1** and **2** have been characterized by physico-chemical and spectroscopic tools, and **1** has been structurally characterized by single-crystal X-ray crystallography. The electrochemical behavior of the complexes shows the Ru(III)/Ru(II) couple at different potentials with *quasi*-reversible voltammograms. The interaction of these complexes with calf thymus DNA by using absorption and emission spectral studies allowed determination of the binding constant K_b and the linear Stern–Volmer quenching constant K_{SV}.

Keywords: Ruthenium(II) complexes; Benzimidazole; Quinazoline derivatives; Crystal structure; DNA-binding

1. Introduction

Nitrogen heterocyclics bearing benzimidazole and also quinazoline derivatives often reveal interesting biological and pharmaceutical activities [1–7]. Recently, several polycyclic DNA-targeting agents having a quinazoline planar fragment have been shown to be cytotoxic and have superior antitumor activity over kinase inhibitors [8]. These compounds interact with double stranded DNA and also present selective recognition of DNA sequences. Although medicinal chemistry is predominately focused on design of organic molecules, there is increasing interest toward the design of metal-based therapeutic and diagnostic agents [9–12]. Such metal–ligand assemblies allow convergent synthetic approaches and give access to structural motifs that differ from purely organic molecules.

*Corresponding author. Email: pabitracc@yahoo.com

ISSN 0095-8972 print/ISSN 1029-0389 online
http://dx.doi.org/10.1080/00958972.2012.667807

Owing to the spectroscopic and redox properties of ruthenium(II) complexes with heterocyclic N-donor ligands, the study of their interaction with proteins, DNA, and lipids have received considerable attention for applications in biochemistry and clinical diagnosis [13–16]. Moreover, six-coordinate ruthenium complexes are good scaffolds as ruthenium is kinetically inert and forms compounds that display properties and stabilities comparable to purely organic molecules [17].

Continuing our ongoing interest to interaction of metal chelates with calf thymus DNA (CT-DNA) [18–22], herein we report the synthesis, characterization, and DNA-binding study of two ruthenium(II) complexes of heterocyclic ligands resulting from a benzimidazole-based quinazoline derivative (**L**). The complexes were characterized by physico-chemical and spectroscopic tools and the solid state structure of **1** have been established by single-crystal X-ray crystallography. Redox behavior of these complexes in acetonitrile by cyclic voltammetry (CV) and the interaction with CT-DNA have also been studied.

2. Experimental

2.1. *Materials and physical measurements*

All chemicals and reagents were obtained from commercial sources and used as received. Solvents were distilled from an appropriate drying agent. $RuCl_3 \cdot 3H_2O$ (Aldrich) was used without purification. *cis*-$[Ru^{II}Cl_2(dmso)_4]$ was synthesized according to the literature method [23]. Tetra-*n*-butylammonium perchlorate (TBAP) was prepared by addition of sodium perchlorate (taking the usual precaution for handling perchlorate salts!) to a hot solution of tetra-*n*-butylammoniumbromide (Aldrich). Commercially available silica gel (60–120 mesh) from SRL was used for chromatographic separation. The products were recrystallized from aqueous ethanol.

C, H, and N elemental analyses were performed on a Perkin Elmer model 2400 elemental analyzer and ruthenium analyses were carried out with a Varian atomic absorption spectrophotometer model-AA55B, GTA using a graphite furnace. Electronic absorption spectra were recorded on a JASCO UV-Vis/NIR spectrophotometer model V-570 from 1100 to 200 nm. IR spectra (KBr discs, 4000–300 cm^{-1}) were recorded using a Perkin-Elmer FTIR model RX1 spectrometer. ^1H NMR spectra were recorded on a Bruker AC300 spectrometer using TMS as internal standard in $CDCl_3$. Room temperature magnetic susceptibility measurements were performed with a vibrating sample magnetometer PAR 155 model. Molar conductances (Λ_M) were measured in a Systronics conductivity meter (model 304) in acetonitrile with $\sim 10^{-3}$ mol L^{-1}. The measurement of pH of the reaction mixture was done with a Systronics digital pH meter (Model 335). Electrochemical measurements were recorded on a CH-instrument electrochemical system (Model 620D) using Pt-wire and Ag/AgCl as working and reference electrodes, respectively, with TBAP as supporting electrolyte. All the measurements were made at 298 K by using 10^{-3}–10^{-4} mol L^{-1} in acetonitrile purged with dry nitrogen for 3–4 min in order to remove dissolved oxygen.

2.2. *Preparation of quinazoline derivatives*

[6-(2-pyridinyl)-5,6-dihydrobenzimidazo[1,2-c]quinazoline] (**L**): An ethanolic solution of 2-(2-aminophenyl)benzimidazole (2.09 g, 10.0 mmol) was added to pyridine-2-carboxaldehyde (1.07 g, 10.0 mmol) in ethanol (25 mL) at room temperature and the mixture was allowed to reflux for 4 h. A white crystalline precipitate of **L** was obtained from the yellow solution through slow evaporation of the solvent. Single crystals of **L** suitable for X-ray crystallography were obtained from a methanolic solution of the white product on slow evaporation at room temperature.

$C_{19}H_{14}N_4$: Anal. Found: C, 76.56; H, 4.75; N, 18.49; Calcd: C, 76.48; H, 4.73; N, 18.78; m.p. 231 ± 1°C. Yield: 90%. MS: $[M+H]^+$, *m/z,* 299.3; IR (KBr, cm^{-1}): $\nu_{N-H,}$ 2950, $\nu_{C=N,}$ 1477. ^1H NMR (*δ,* ppm in DMSO-d_6): 8.44 (d, 1H, $J=3.9$); 7.91 (d, 1H, $J=7.2$); 7.77–7.70 (m, 2H); 7.63 (d, 1H, $J=7.2$); 7.35–7.10 (m, 7H); 6.85–6.77 (m, 2H).

6-pyridin-yl-benzo[4,5]imidazo[1,2-c]quinazoline ($\mathbf{L^2}$): The synthesis of $\mathbf{L^2}$ was carried out by oxidation of **L** following the literature method [24]. $KMnO_4$ (0.5 g) was added to 0.298 g of **L** in dry acetone (100 mL) and allowed to reflux for 6 h. The resulting mixture was filtered and the solid mass obtained from this filtrate was poured into water (50 mL) and then extracted by chloroform (2 × 25 mL). Anhydrous sodium sulfate was added to the organic species and then filtered after vigorous stirring of the mixture. The filtrate was dried in a rotary evaporator giving $\mathbf{L^2}$ as white solid.

$C_{19}H_{12}N_4$ ($\mathbf{L^2}$): Anal. Found: C, 77.19; H, 4.05; N, 18.76; Calcd: C, 77.01; H, 4.09; N, 18.91; m.p. 211 ± 1°C. Yield: 97%. MS: $[M+H]^+$, *m/z*, 297.3; IR (KBr, cm^{-1}): $\nu_{C=N,}$ 1477. ^1H NMR (*δ*, ppm in $CDCl_3$): 8.85 (d, 1H, $J=4.8$); 8.74 (d, 1H, $J=7.8$); 8.08–7.92 (m, 4H); 7.80–7.60 (m, 3H); 7.45 (t, 1H, $J=7.2$); 7.12 (t, 1H, $J=7.2$); 6.54 (d, 1H, $J=8.4$).

2.3. *Preparation of ruthenium(II) complexes*

Synthesis of *fac*-[$Ru(L^1)_2$] (**1**): To the ethanolic solution of **L** (0.298 g, 1.0 mmol), a solution of *cis*-[$RuCl_2(dmso)_4$] (0.242 g, 0.5 mmol) in dry EtOH (20 mL) previously purged with N_2 was added dropwise and the resulting solution was stirred for 6 h under N_2. The solvent was evaporated off and the solid mass dissolved in the minimum amount of dichloromethane and chromatographed over a silica gel column prepared in dichloromethane. The first band was washed out by CH_2Cl_2–MeOH (9 : 1) while the blue band was collected through the column with a 3 : 1 solvent mixture of CH_2Cl_2–MeOH to isolate *fac*-[$Ru(L^1)_2$] isomer.

fac-[$Ru(L^1)_2$] (**1**): $C_{38}H_{26}N_8Ru$: Anal. Found: C, 65.60; H, 3.44; N, 16.11; Ru, 14.34; Calcd: C, 65.12; H, 3.37; N, 15.98; Ru, 14.50. Yield: 70–72%. IR (cm^{-1}): $\nu_{C=N,}$ 1472; Conductance Λo ($\Omega^{-1}\,cm^2\,mol^{-1}$) in methanol: 52. ^1H NMR (*δ,* ppm in CD_3OD): 8.78 (s, 2H), 8.73 (d, 2H, $J=5.1$), 8.20 (d, 2H, $J=7.2$), 7.86 (d, 2H, $J=7.8$), 7.51 (m, 8H), 7.16 (m, 6H), 7.05 (d, 2H, $J=5.4$), 6.78 (t, 2H, $J=7.5$). ESI-MS (*m/z*): $[M+Na]^+$, 718.0 (10% abundance).

Synthesis of *trans*-[$RuCl_2(L^2)_2$] (**2**): Nitrogen was bubbled in a brown solution of $RuCl_3 \cdot 3H_2O$ (0.130 g, 0.5 mmol) in dry tetrahydrofuran (THF) (10 mL). Then 0.298 g (1.0 mmol) of **L** in 20 mL of THF (previously purged with N_2) was added, refluxing the mixture for 2 h under N_2. During this process the color turned into green with a precipitate. The solution was cooled to room temperature and the green solid was

collected through filtration, followed by washing thoroughly with water, ethanol, and finally diethylether. It was then dried in a vacuum desiccator over P_4O_{10}. Yield: 80–82%.

A parallel reaction was performed with reactants in same mole ratio in dry ethanol. Here, the solution mixture of $\mathbf{L^2}$ (0.296 g, 1.0 mmol) and $RuCl_3 \cdot 3H_2O$ (0.130 g, 0.5 mmol) in 25 mL of dry ethanol was refluxed for 4 h under N_2. The reaction proceeded in the same way and the green precipitate was collected and dried as above. Yield: 80–84%.

trans-$[RuCl_2(L^2)_2]$ (**2**): $C_{38}H_{24}N_8Cl_2Ru$: Anal. Found: C, 59.12; H, 3.26; N, 14.53; Ru, 13.33; Calcd: C, 59.69; H, 3.16; N, 14.65; Ru, 13.22. Yield: 80%. Conductance Λo ($\Omega^{-1}\,cm^2\,mol^{-1}$) in methanol: 68. IR ($cm^{-1}$): $\nu_{C=N,}$ 1471; $\nu_{Ru-Cl,}$ 342; ^1H NMR (δ, ppm in $CDCl_3$): 8.52 (d, 1H, $J = 3.1$); 8.14 (d, 1H, $J = 7.1$); 7.85 (d, 1H, $J = 8.2$); 7.46 (t, 1H, $J = 7.4$); 7.30 (t, 1H, $J = 7.2$); 7.21–7.06 (m, 3H); 6.83–6.73 (m, 4H). ESI-MS (m/z): $[M + Na]^+$, 787.1 (10% abundance).

2.4. *X-ray crystal structure analysis*

Diffraction data of **L** and **1** were measured with Mo-Kα radiation ($\lambda = 0.71073$ Å) at 293 K on a Marresearch Image plate diffractometer. The crystals were positioned at 70 mm from the image plate and 95 frames were measured at 2° intervals with a counting time of 2 min. Analysis of data sets was carried out with the XDS program [25].

The structures were solved with direct methods [26] and refined by full-matrix least-squares based on F^2 with all observed reflections [26]. Six residuals were interpreted as oxygen of water (two of these refined with half occupancy). Hydrogen atoms at carbons were included at geometric positions with thermal parameters = 1.2 times that of the associated carbon, while those of water molecules were located on ΔF map and refined with distance constraints. An empirical absorption correction was applied to **1** using DIFABS [27]. Crystal data and details of refinement are reported in table 1.

2.5. *DNA-binding experiments*

The tris-HCl buffer solution (pH 7.4), used in all the experiments involving CT-DNA, was prepared using deionized and sonicated HPLC grade water (Merck). The used CT-DNA was sufficiently free from protein with the ratio of UV absorbance of the DNA in tris-HCl solution at 260 and 280 nm (A260/A280) of *ca* 1.9 [28]. The concentration of DNA was determined with the help of its extinction coefficient ε of 6600 $L\,mol^{-1}\,cm^{-1}$ at 260 nm [29]. The stock solution of DNA was always stored at 4°C and used within 4 days. Concentrated stock solution of complex was prepared by dissolving the ruthenium(II) complex in DMSO and suitably diluting with tris-HCl buffer to the concentration required for all experiments. Absorption spectral titration was performed by keeping constant the concentration of ruthenium(II) complex while varying the CT-DNA concentration. To eliminate the absorbance of DNA itself, an equal solution of CT-DNA was added to the ruthenium(II) complex solution and to the reference.

In fluorescence displacement experiment with ethidium bromide (EB), 5 µL of EB solution (1.0 mmol L^{-1}) in tris-HCl were added to 1.0 mL of DNA solution at saturated binding levels [30] and stored in the dark for 2.0 h. The ruthenium(II) complex solution

Table 1. Crystal data and details of refinement for $\mathbf{1} \cdot 5H_2O$.

Empirical formula	$C_{38}H_{26}N_8Ru \cdot 5H_2O$
Formula weight	785.82
Crystal system	Monoclinic
Space group	$P2_1/c$
Unit cell dimensions (Å, °)	
a	16.351(18)
b	12.645(14)
c	17.578(19)
α	90.00
β	92.50(1)
γ	90.00
Volume (Å^3), Z	3631(7), 4
Calculated density (g cm^{-3})	1.438
Absorption coefficient (mm^{-1})	0.487
$F(000)$	1616
θ range for data collection (°)	1.98–26.00
Collected/unique reflections	20,544/6672
Reflections [$I > 2\sigma(I)$]	3120
Parameters	514
Goodness-of-fit on F^2	0.928
Final R indices [$I > 2\sigma(I)$]	$R_1 = 0.0736$, $wR_2 = 0.1006$
R indices (all data)	$R_1 = 0.1243$, $wR_2 = 0.1814$
Largest difference peak and hole (e Å^{-3})	0.432 and −0.453

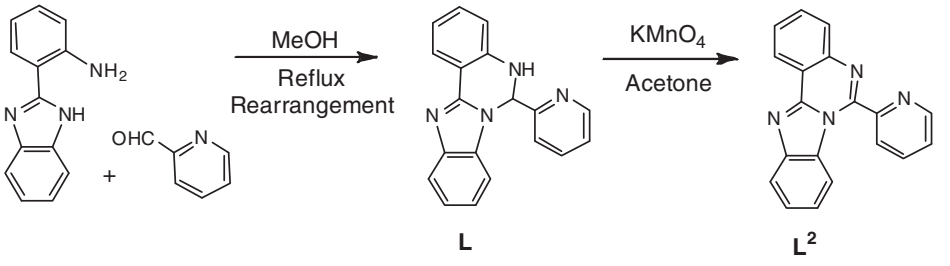

Scheme 1. Synthetic procedure of organic moieties.

was titrated into the DNA/EB mixture and then diluted in tris-HCl buffer to 5.0 mL, making solutions with varied mole ratio of the metal complex to CT-DNA. Prior to measurements, the mixture was shaken and incubated at room temperature for 30 min. The fluorescence spectra of EB bound to DNA were obtained at an emission wavelength of 584 nm.

3. Results and discussion

3.1. *Syntheses*

L was synthesized by refluxing 2-(2-aminophenyl)benzimidazole and pyridine-2-carboxaldehyde in equimolar ratio in methanol (scheme 1), giving white

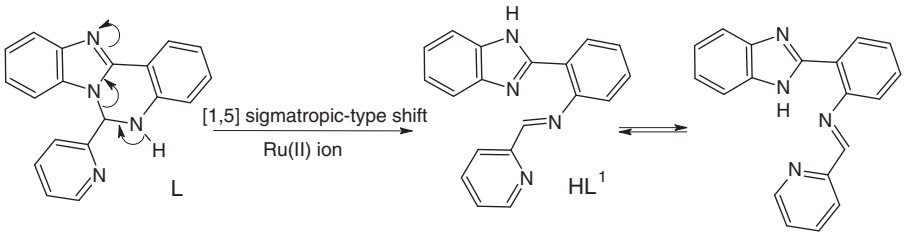

Scheme 2. [1,5] Sigmatropic-type shift of **L**.

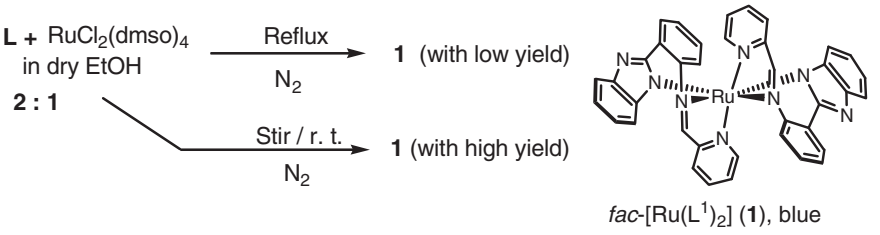

Scheme 3. Synthetic strategy for **1**.

[6-(2-pyridinyl)-5,6-dihydrobenzimidazo[1,2-c]quinazoline] as product. Structural analysis by spectroscopic tools and X-ray diffraction confirmed the cyclic rearranged product. On reaction with $KMnO_4$ in acetone, **L** is converted to its oxidized product, 6-pyridin-yl-benzo[4,5]imidazo[1,2-c]quinazoline ($\mathbf{L^2}$).

During the reaction with ruthenium(II) a [1,5] sigmatropic-type shift of **L** occurred prior to metal coordination (scheme 2), giving *in situ* $\mathbf{HL^1}$ [31] which behaved as a tridentate monobasic ligand to form $[Ru(L^1)_2]$ (**1**). The synthetic procedure of **1** is shown in scheme 3. When the reaction was conducted with 1 : 2 molar ratio of *cis*-$[RuCl_2(dmso)_4]$ and **L** in ethanol at reflux, **1** was obtained with low yield, but on stirring the reaction mixture of *cis*-$[RuCl_2(dmso)_4]$ and **L** (same solvent and molar ratio) at ambient temperature the yield of **1** was significantly improved. The blue band corresponding to pure *fac*-isomer **1** was eluted by mixture of CH_2Cl_2–MeOH (3 : 1) from the silica gel column and charged with the resulting solid mass of the reaction mixture between *cis*-$[RuCl_2(dmso)_4]$ and **L** in 1 : 2 mole ratio at room temperature.

Reaction of **L** with $RuCl_3$ in dry THF under dinitrogen afforded a ruthenium(II) complex $[RuCl_2(L^2)_2]$ (**2**) *via* spontaneous reductive chelation of ruthenium and concomitant oxidation of **L** to $\mathbf{L^2}$. From the cooled reaction mixture, green crystalline compound was obtained in high yield. The same **2** was directly obtained when $\mathbf{L^2}$ reacts with $RuCl_3 \cdot 3H_2O$ in ethanol *via* spontaneous reduction of Ru(III) by the solvent (scheme 4).

Microanalytical data confirm the formulation of **1** and **2**. Conductivity measurements indicate that both ruthenium(II) complexes are non-electrolytes in methanolic solution, and the magnetic moment studies demonstrate the complexes are diamagnetic.

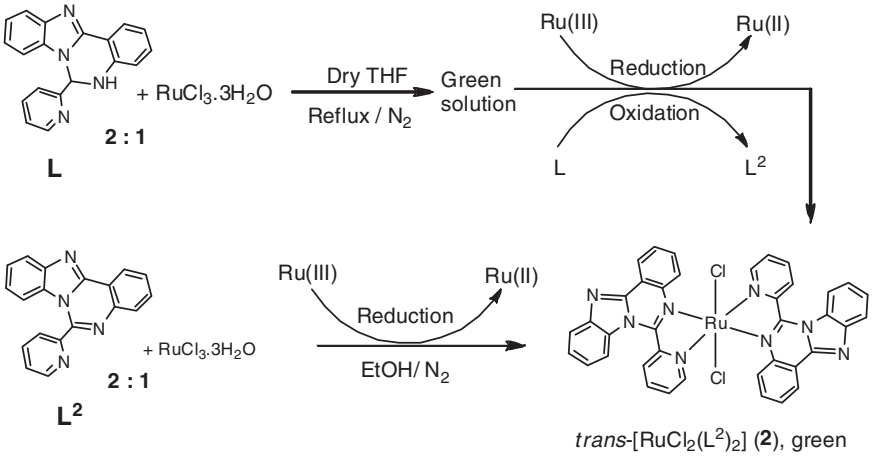

Scheme 4. Synthetic methodologies of **2**.

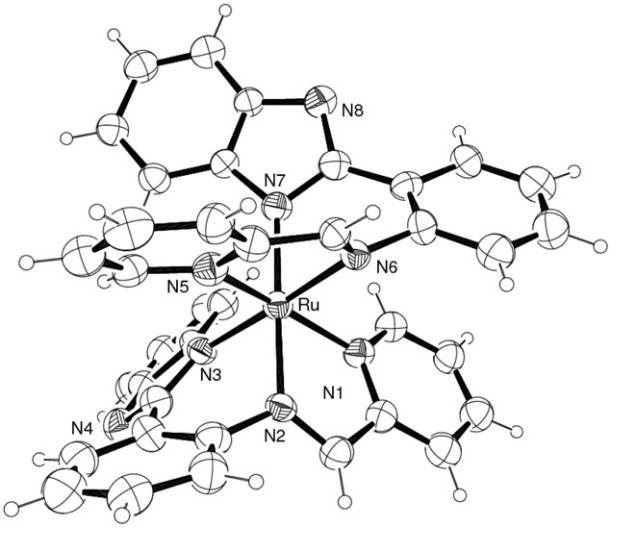

Figure 1. Solid state structure of $[Ru(L^1)_2]$ (**1**) with ellipsoids at 35% probability.

3.2. *Structural characterization*

Since the X-ray diffraction analysis of **L** has already been reported [32], its molecular structure will be not described here; figure S1 and crystal data have been included as "Supplementary material."

The ORTEP view of **1** is illustrated in figure 1, and a selection of bond distances and angles are listed in table 2. The complex has approximate C_2 symmetry with the two-fold axis bisecting the angles subtended at Ru by pyrrolic nitrogen atoms and imine nitrogen atoms (almost normal to picture of scheme 3). The metal ion, in a distorted

Table 2. Selected bond lengths (Å) and angles (°) of **1**.

Ru–N(1)	2.074(5)	Ru–N(5)	2.045(6)
Ru–N(2)	1.968(5)	Ru–N(6)	2.004(5)
Ru–N(3)	2.048(5)	Ru–N(7)	2.059(5)
N(1)–Ru–N(2)	76.9(2)	N(2)–Ru–N(7)	177.8(2)
N(1)–Ru–N(3)	93.5(2)	N(3)–Ru–N(5)	98.7(2)
N(1)–Ru–N(5)	160.8(2)	N(3)–Ru–N(6)	177.4(2)
N(1)–Ru–N(6)	89.2(2)	N(3)–Ru–N(7)	98.2(2)
N(1)–Ru–N(7)	101.0(2)	N(5)–Ru–N(6)	78.7(2)
N(2)–Ru–N(3)	81.4(2)	N(5)–Ru–N(7)	91.9(2)
N(2)–Ru–N(5)	90.2(2)	N(6)–Ru–N(7)	81.4(2)
N(2)–Ru–N(6)	99.2(2)		

octahedral geometry, has a N_6 chromophore from nitrogen atoms of two tridentate ligands coordinating *facial*. Ru–N bond distances range from 1.968(5) to 2.074(5) Å. Making allowance for the esd's, the Ru–N(py) bonds, *trans* to each other, are slightly different (2.074(5) and 2.045(6) Å), while the *cis* located Ru–N(pyrrole) ones of 2.048(5) and 2.059(5) Å are more comparable. The significant difference between Ru–N(imino) bonds of 1.968(5) and 2.004(5) Å are mainly due to ligand geometrical requirements in order to accomplish a strain coordination from six- and a five-membered rings. Distortions in bond angles are clearly evidenced by the N(py)–Ru–N(py) angle of 160.8(2)°, while the other N–Ru–N angles, of *trans* donors, are 177.8(2)° and 177.4(2)°, closer to ideal octahedral. The variability in coordination bond distances, imputable also to the different nature of N-donors, are detected in other Ru complexes [33, 34]. The conformation of the tridentate ligands are comparable, with torsion angle about the C=N imino bond of 160.9° and 159.5°.

The metal complexes stack along the [100] direction connecting by π–π interactions occurring between benzimidazole phenyl moieties related by inversion centers (centroid-to-centroid distance of *ca* 3.6 Å). The crystallographic analysis revealed the presence of six residuals interpreted as water molecules (two at half occupancy, thus five per complex unit) and these lattice molecules fill channels outlined by the complexes and running parallel to the crystallographic axis *a* (figure 2). These water molecules are connected through H-bonds, the shortest distance being 2.47 Å between O(4w) and O(5w), and two of these weakly appended to the uncoordinated benzimidazole nitrogen (O(1w)···N(8) 3.065(7) Å; O(3w)···N(4) 2.998(8) Å).

3.3. *Spectral characterization*

The IR spectrum of **L** showed a characteristic band at ~2950 cm^{-1} for $\nu_{N-H,}$ which is absent in the spectra of the ruthenium(II) complexes and in 6-pyridin-yl-benzo[4,5]imidazo[1,2-c]quinazoline (**L^2**). The $\nu_{C=N}$ band in **L** is 1477 cm^{-1}, shifted to lower wavenumbers in the complexes, suggesting coordination. The green complex $[Ru(L^2)_2Cl_2]$ (**2**) displays a sharp, single stretch at 342 cm^{-1} attributable to ν_{Ru-Cl} [35], indicating chlorines bound to ruthenium(II) *trans* [33].

The ^{1}H NMR spectra have been recorded in deuterated solvents. Signals for **L** and **L^2** appeared in the spectra supporting the proposed structural formulas. Integration of proton signals clearly indicates the lack of two-protons in **L^2** in comparison to **L**.

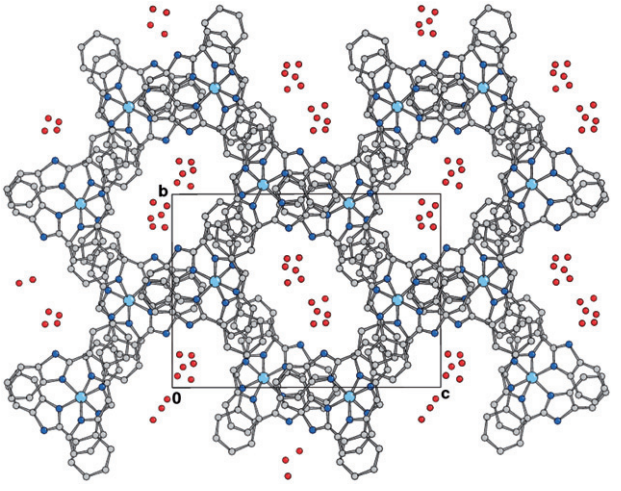

Figure 2. Crystal packing of **1** viewed down the *a*-axis showing the channel filled by lattice water molecules.

Table 3. UV-Vis spectral data and electrochemical data.[a]

Compound	λ nm (ε) (ε, $dm^3 mol^{-1} cm^{-1}$)	Electrochemical data $E_{1/2}$, ΔE (V)
1	581 (3572), 293 (16,462), 239 (16,126)	0.91 (0.105)
2	598 (3563), 298 (29,708), 237 (28,245)	1.11 (0.084)

[a]In acetonitrile.

This spectral study and mass spectra ($[M+H]^+$, m/z 299.34 for **L** and m/z 297.34 for $\mathbf{L^2}$) support the proposed structures for **L** and $\mathbf{L^2}$.

In the ^{1}H NMR spectrum of **1** protons are in accord with the proposed structure. A new singlet (at 8.783 ppm) assignable for CH attached to the imine-N corresponding to the azomethine (CH=N) is present in $[Ru(L^1)_2]$ (**1**). This peak was absent in the ^{1}H NMR spectrum of **L** and its singlet nature indicates a similar electronic environment of both azomethine protons. The peak at $m/z = 718$ (10% abundance) along with other peaks in the ESI-MS spectrum of **1** gives evidence the existences of $[M+Na]^+$.

The signals of the protons of **2** are similar with those of $\mathbf{L^2}$ but at relatively high field compared to those in free $\mathbf{L^2}$. This may be due to the presence of two coordinated chlorides *trans* in the coordination sphere of ruthenium. Here the peak of azomethine proton observed in **1** was not detected. The peak at $m/z = 787.0544$ with 10% abundance along with other peaks in the ESI-MS spectrum corresponds to the $[M+Na]^+$ ion (where M = formula weight of **2**).

Electronic absorption spectra of all the complexes were recorded at room temperature using acetonitrile as the solvent and data are listed in table 3. The spectra of the complexes exhibit the characteristic transitions at 237–239 nm and 293–298 nm corresponding to intramolecular $\pi \rightarrow \pi^*$ and $n \rightarrow \pi^*$ transitions, respectively. The bands at 581 and 598 nm in **1** and **2**, respectively, were observed due to the d(Ru) $\rightarrow \pi^*$ (ligand) MLCT transitions.

3.4. *Electrochemical behavior*

Electrochemical properties of **1** and **2** have been studied by CV on a Pt working electrode in MeCN from −2.0 to +2.0 V at 25°C. Each complex exhibits a redox wave ($E_{1/2}$: **1**, 0.91; **2**, 1.11 V *vs.* Ag/AgCl) (table 3) assignable to the Ru(II)/Ru(III) couple. On recording the cyclic voltammetric responses at different scan rates (50–400 mV), the plot of i_{pa} *versus* $\nu^{1/2}$ gave a straight line passing through the origin in each case.

Linearity of these plots [36] indicates that the redox processes occurring at the electrode are diffusion controlled. The peak potential separations ΔE_p (84–105 mV) are generally larger than the ideal Nernstian value of 59 mV for a one-electron transfer, but commonly observed for complexes of this type, apparently due to uncompensated solution resistance. The high anodic potential for the Ru(III)/Ru(II) couple for green **2** in comparison to that of the blue **1** is due to strong π-acceptor property of $\mathbf{L^2}$ (obtained from **L** by oxidation) compared to $\mathbf{L^1}$. This electrochemical behavior of the ruthenium ion is in agreement with the electronic property of the ligand.

3.5. *DNA-binding studies*

3.5.1. Electronic absorption titration. To examine the binding of ruthenium(II) complexes with DNA, the absorption spectra of the complexes were recorded during titration with CT-DNA. As shown in figure 3, spectra indicate a significant hyperchromism centered around 300 nm, suggesting a strong interaction between the ruthenium(II) complexes and DNA. The spectral change might be interpreted as due to groove binding of the adducts [37], since ruthenium(II) complexes containing fused polyaromatic systems having coplanar atoms (organic ligand) facilitates formation of van der Waals contacts or hydrogen bonds during interaction with DNA grooves. From these titration data the intrinsic binding constants (K_b) of the complexes with CT-DNA have been determined using the following equation [38]:

$$[\mathrm{DNA}]/(\varepsilon_a - \varepsilon_f) = [\mathrm{DNA}]/(\varepsilon_b - \varepsilon_f) + 1/[K_b(\varepsilon_b - \varepsilon_f)],$$

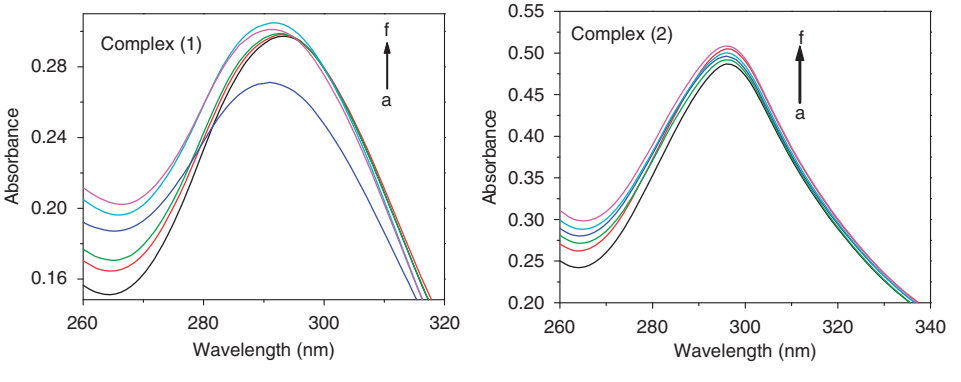

Figure 3. Electronic spectra of **1** and **2** through titration with CT-DNA in tris-HCl buffer; (**1**) = 1.60×10^{-5} mol L^{-1}; (**2**) = 1.31×10^{-5} mol L^{-1}; [DNA]: (a) 0.0, (b) 2.0×10^{-6}, (c) 4.00×10^{-6}, (d) 6.0×10^{-6}, (e) 8.0×10^{-6}, and (f) 1.0×10^{-5} mol L^{-1}. The increase in DNA concentration is indicated by an arrow.

where [DNA] represents the DNA concentration, ε_f and ε_b are the extinction coefficients for the free and fully bound ruthenium(II) complex, respectively, and ε_a the metal complex extinction coefficient during each addition of DNA. The [DNA]/($\varepsilon_a - \varepsilon_f$) plot against [DNA] gave a linear relationship (figure 4). The intrinsic binding constants (K_b) for the complexes were calculated from the slope to intercept ratio and reported in table 4. These values are in agreement with those of well-established groove binding rather than classical intercalation [39].

3.5.2. Ethidium bromide fluorescence displacement experiments. EB fluorescence displacement experiments were also performed to investigate the interaction mode of the complex with CT-DNA. In fact EB fluorescence intensity will be enhanced in the presence of DNA because of its intercalation into the helix, and it was quenched by addition of another molecule that displaces EB from DNA [40]. Here, the significant decreases of the fluorescence intensity of EB bound to DNA at 620 nm were recorded by increasing the concentration of the complexes as shown in figures 5(i) and 6(i). The observation of EB fluorescence quenching due to the releasing of some EB molecules from the EB-DNA system is supportive to the interaction of the ruthenium(II) complexes with CT-DNA through groove binding. Here the quenching of EB bound to

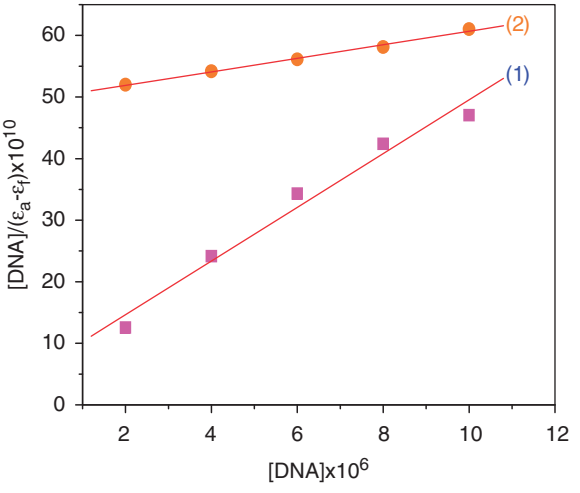

Figure 4. Plot of [DNA]/($\varepsilon_a - \varepsilon_f$) *vs.* [DNA] for titration of CT-DNA with **1** and **2** in tris-HCL buffer; for **1** binding constant $K_b = 7.381 \times 10^5$ $(\text{mol L}^{-1})^{-1}$ ($R = 0.98811$, $n = 5$ points); for **2** $K_b = 0.221 \times 10^5$ $(\text{mol L}^{-1})^{-1}$ ($R = 0.99674$, $n = 5$ points).

Table 4. DNA experiment K_b and K_{sv} values for complexes.

Entry	Compound	K_b $((\text{mol L}^{-1})^{-1})$	K_{SV}
1	*fac*-[Ru(L^1)$_2$] (**1**)	7.381×10^5	1.745×10^4
2	*trans*-[RuCl$_2$(L^2)$_2$] (**2**)	0.221×10^5	0.393×10^4

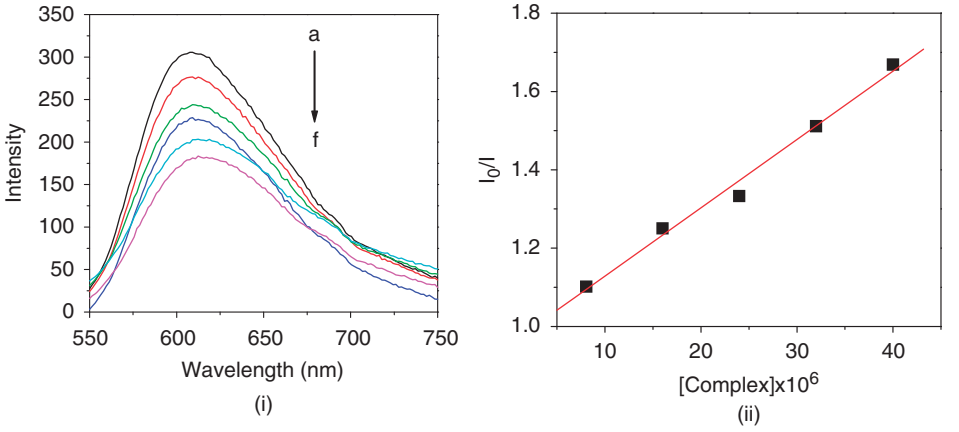

Figure 5. (i) Emission spectra of CT-DNA–EB system in tris-HCl buffer based on the titration of **1**. $\lambda_{ex} = 522$ nm; [EB] $= 0.96 \times 10^{-6}$ mol L^{-1}; [DNA] $= 0.1 \times 10^{-4}$; [Complex]: (a) 0.0, (b) 8.05×10^{-6}, (c) 1.6×10^{-5}, (d) 2.4×10^{-5}, (e) 3.2×10^{-5}, and (f) 4.0×10^{-5} mol L^{-1}. (ii) Plot of I_0/I *vs.* [complex] for titration of CT-DNA–EB system; Stern–Volmer quenching constant $K_{sv} = 1.745 \times 10^4$ (R = 0.99433, $n = 5$ points).

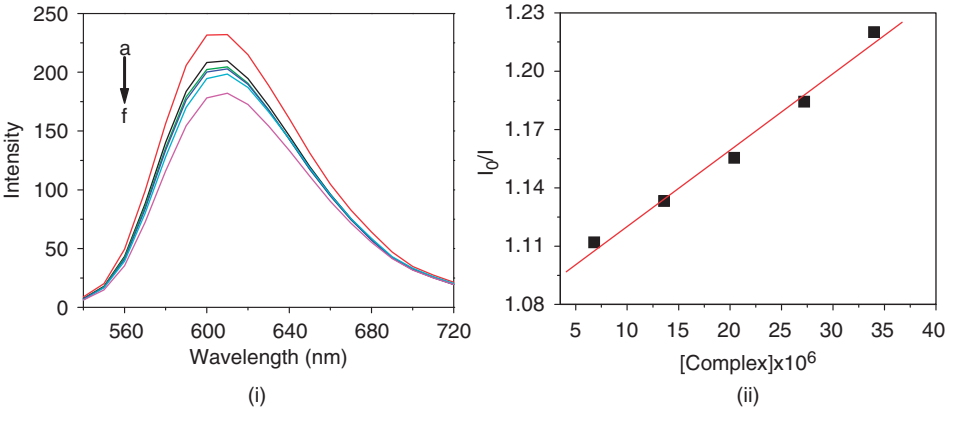

Figure 6. (i) Emission spectra of CT-DNA–EB system in tris-HCl buffer based on the titration of **2**. $\lambda_{ex} = 522$ nm; [EB] $= 0.96 \times 10^{-6}$ mol L^{-1}; [DNA] $= 0.1 \times 10^{-4}$ mol L^{-1}; [Complex]: (a) 0.0, (b) 6.81×10^{-6}, (c) 1.36×10^{-5}, (d) 2.04×10^{-5}, (e) 2.72×10^{-5}, and (f) 3.4×10^{-5} mol L^{-1}. (ii) Plot of I_0/I *vs.* [complex] for titration of CT-DNA–EB system; Stern–Volmer quenching constant $K_{SV} = 0.393 \times 10^4$ (R = 0.99336, $n = 5$ points).

DNA by the ruthenium(II) complexes is in agreement with the linear Stern–Volmer equation:

$$I_0/I = 1 + K_{SV}[\text{complex}],$$

where I_0 and I represent the fluorescence intensities in the absence and presence of quencher, respectively. K_{SV} is the linear Stern–Volmer quenching constant and [complex] the molar concentration of the quencher. From the slope of the regression

line in the derived plot of I_0/I *versus* [complex] (figures 5(ii) and 6(ii)), the K_{SV} values for the complexes were determined as 1.745×10^4 for **1** ($R = 0.99433$, $n = 5$ points) and 0.393×10^4 for **2** ($R = 0.99336$, $n = 5$ points), indicating a strong affinity of ruthenium(II) complexes to CT-DNA.

From these DNA-binding studies, the trends of K_{SV} and K_b are of same order. The K_{SV} values obtained in this study increase with increasing values of K_b, indicating the same mode of interactions of the ruthenium(II) complexes with CT-DNA.

4. Conclusion

The reaction of [6-(2-pyridinyl)-5,6-dihydrobenzimidazo[1,2-c]quinazoline] (**L**) with *cis*-$[RuCl_2(dmso)_4]$ led to the formation of a blue complex $[Ru(L^1)_2]$ (**1**) as **L** changed to [2-(1H-benzoimidazol-2-yl)-phenyl]-pyridin-2-ylmethylene-amine (**HL^1**) *via* a [1,5] sigmatropic shift *in situ*. In reaction with $RuCl_3 \cdot 3H_2O$, **L** got oxidized to 6-pyridin-yl-benzo[4,5]imidazo[1,2-c]quinazoline (**L^2**) isolating green *trans*-$[RuCl_2(L^2)_2]$ (**2**), which could also be obtained from the reaction of $RuCl_3$ with **L^2**. The crystal structure of **1** shows tridentate **L^1** coordinating ruthenium(II) with facial configuration. Both complexes interact with CT-DNA through groove binding, but **1** exhibits a higher binding constant ($K_b = 7.38 \times 10^5$ $(mol\,L^{-1})^{-1}$) with respect to **2** (0.221×10^5 $(mol\,L^{-1})^{-1}$). The K_b of **1** is comparable to that ($K_b = 7.2 \times 10^5$ $(mol\,L^{-1})^{-1}$) of the reported water-soluble $[Ru(MeIm)_4(tip)]^{2+}$, MeIm = 1-methylimidazole, tip = 2-(thiophene-2-group)-1H-imidazo[4,5-f][1,10]phenanthroline) [41]. But, K_b of **2** is comparable to that ($K_b = 2.3$–3.3×10^4 $(mol\,L^{-1})^{-1}$) of $[Ru(dmp)_2(APIP)]^{2+}$ (dmp = 2,9-dimethyl-1,10-phenanthroline, APIP = 2-(2-aminophenyl)imidazo[4,5-f][1,10]phenanthroline) [42] suggesting that **2** binds to CT-DNA in partial intercalation, with π–π stacking on the DNA surface [43].

Supplementary material

Crystallographic data for **1** and **L** have been deposited with the Cambridge Crystallographic Data Centre, CCDC Nos 651979 and 651980, respectively. The data can be obtained free of charge *via* http://www.ccdc.cam.ac.uk/conts/retrieving.html, or from the Cambridge Crystallographic Data Centre, 12 Union Road, Cambridge CB2 1EZ, UK; Fax: (+44) 1223-336-033; or E-mail: deposit@ccdc.cam.ac.uk

Acknowledgments

Financial support from Department of Science and Technology, New Delhi, India is gratefully acknowledged. We thank EPSRC (UK) and the University of Reading for funds for the Image Plate.

References

[1] J.J. Marugan, W. Zheng, O. Motabar, N. Southall, E. Goldin, W. Westbroek, B.K. Stubblefield, E. Sidransky, R.A. Aungst, W.A. Lea, A. Simeonov, W. Leister, C.P. Austin. *J. Med. Chem.*, **54**, 1033 (2011).
[2] A.A. Smith, K.S. Ibrahim, S. Parimalakrishnan, A.K. Muthu, P. Muthumani. *Quart. J. Appl. Chem.*, **4**, 7 (2008).
[3] S. Ozden, D. Atabey, S. Yildz, H. Goker. *Bioorg. Med. Chem.*, **13**, 1587 (2005).
[4] C. Kus, G. Ayhan-Kilcigil, B. Can-Eke, M. Iscan. *Arch. Pharm. Res.*, **27**, 156 (2004).
[5] M. Ranson, S. Wardell. *J. Clin. Pharm. Ther.*, **29**, 95 (2004).
[6] W.A. Denny. *Farmaco*, **56**, 51 (2001).
[7] J.P. Karwowski, M. Jackson, R.R. Rasmussen, P.E. Humphrey, J.B. Poddig, W.L. Kohl, M.H. Scherr, S. Kadam, J.B. McAlpine. *J. Antibiot.*, **46**, 374 (1993).
[8] A. Garofalo, L. Goossens, B. Baldeyrou, A. Lemoine, S. Ravez, P. Six, M.-H. David-Cordonnier, J.-P. Bonte, P. Depreux, A. Lansiaux, J.-F. Goossens. *J. Med. Chem.*, **53**, 8089 (2010), and references therein.
[9] H.-K. Liu, P.J. Sadler. *Acc. Chem. Res.*, **44**, 349 (2011).
[10] N. Farrell. *Coord. Chem. Rev.*, **232**, 1 (2002).
[11] C. Orvig, M.J. Abrams. *Chem. Rev.*, **99**, 2201 (1999).
[12] Z. Guo, P.J. Sadler. *Angew. Chem., Int. Ed.*, **38**, 1512 (1999).
[13] M.K. Nazeeruddin, C. Klein, P. Liska, M. Gratzel. *Coord. Chem. Rev.*, **249**, 1460 (2005).
[14] A. Kukrek, D. Wang, Y. Hou, R. Zong, R. Thummel. *Inorg. Chem.*, **45**, 10131 (2006).
[15] P. Wang, C. Klein, R.H. Baker, S.M. Zakeeruddin, M. Gratzel. *J. Am. Chem. Soc.*, **127**, 808 (2005).
[16] Y. Jenkins, A.E. Friedman, N.J. Turro, J.K. Barton. *Biochemistry*, **31**, 10809 (1992).
[17] L. Zhang, P. Carroll, E. Meggers. *Org. Lett.*, **6**, 521 (2004).
[18] S. Sarkar, S. Sen, S. Dey, E. Zangrando, P. Chattopadhyay. *Polyhedron*, **29**, 3157 (2010).
[19] S. Dey, S. Sarkar, H. Paul, E. Zangrando, P. Chattopadhyay. *Polyhedron*, **29**, 1583 (2010).
[20] S. Sarkar, T. Mukherjee, S. Sen, E. Zangrando, P. Chattopadhyay. *J. Mol. Struct.*, **980**, 117 (2010).
[21] S. Dey, T. Mukherjee, S. Sarkar, H.S. Evans, P. Chattopadhyay. *Transition Met. Chem.*, **36**, 631 (2011).
[22] A. Patra, T. Mukherjee, S. Sarkar, E. Zangrando, P. Chattopadhyay. *Polyhedron*, **30**, 2783 (2011).
[23] I.P. Evans, A. Spencer, G. Wilkinson. *J. Chem. Soc., Dalton Trans.*, 204 (1973).
[24] V.R.K. Reddy, S.N. Reddy, C.V. Ratnam. *Synth. Commun.*, **21**, 49 (1991).
[25] W. Kabsch. *J. Appl. Cryst.*, **21**, 916 (1988).
[26] G.M. Sheldrick. *Acta Crystallogr., Sect. A*, **64**, 112 (2008).
[27] N. Walker, D. Stuart. *Acta Crystallogr., Sect. A*, **39**, 158 (1983).
[28] J. Marmur. *J. Mol. Biol.*, **3**, 208 (1961).
[29] M.E. Reichmann, S.A. Rice, C.A. Thomas, P.J. Doty. *J. Am. Chem. Soc.*, **76**, 3047 (1954).
[30] J.K. Barton, J.M. Goldberg, C.V. Kumar, N.J. Turro. *J. Am. Chem. Soc.*, **108**, 2081 (1986).
[31] U.C. Saha, B. Chattopadhyay, K. Dhara, S.K. Mandal, S. Sarkar, A.R. Khuda-Bukhsh, M. Mukherjee, M. Helliwell, P. Chattopadhyay. *Inorg. Chem.*, **50**, 1213 (2011).
[32] K. Jayalakshmi, H.C. Devarajegowda, S.M. Anandalwar, H.G. Bheemanna, V. Gayathri, N.M.N. Gowda, N.S. Begam, K.S. Rangappa, J.S. Prasad. *Anal. Sci.*, **20**, 87 (2004).
[33] T.K. Misra, D. Das, C. Sinha, P. Ghosh, C.K. Pal. *Inorg. Chem.*, **37**, 1672 (1998).
[34] E.C. Constable, A.H. Redondo, C.E. Housecroft, M. Neuburger. *Inorg. Chem. Commun.*, **13**, 70 (2010).
[35] A. Vertova, I. Cucchi, P. Fermo, F. Porta, D.M. Proserpio, S. Rondinini. *Electrochim. Acta*, **52**, 2603 (2007).
[36] R.S. Nicholson, I. Shain. *Anal. Chem.*, **36**, 706 (1964).
[37] R. Vijayalakshmi, M. Kanthimathi, V. Subramanian, B.U. Nair. *Biochem. Biophys. Acta*, **1475**, 157 (2000).
[38] A.M. Pyle, J.P. Rehmann, R. Meshoyrer, C.V. Kumar, N.J. Turro, J.K. Barton. *J. Am. Chem. Soc.*, **111**, 3051 (1989).
[39] L. Strekowski, D.B. Harden, R.L. Wydra, K.D. Stewart, W.D. Wilson. *J. Mol. Recognit.*, **2**, 158 (1989).
[40] R. Indumathy, S. Radhika, M. Kanthimathi, T. Weyhermuller, B.U. Nair. *J. Inorg. Biochem.*, **101**, 434 (2007).
[41] X. Yang, Y. Liu, S. Yao, Y. Xia, Q. Li, W. Zheng, L. Chen, J. Liu. *J. Coord. Chem.*, **64**, 1491 (2011).
[42] Z.-H. Liang, Z.-Z. Li, H.-L. Huang, Y.-J. Liu. *J. Coord. Chem.*, **64**, 3342 (2011).
[43] X.-L. Hong, Z.-H. Liang, M.-H. Zeng. *J. Coord. Chem.*, **64**, 3792 (2011).